**Atmospheric
Chemistry
and Physics**

Summertime photochemistry during CAREBeijing-2007: RO_x budgets and O_3 formation

Z. Liu[1,*], Y. Wang[1], D. Gu[1], C. Zhao[1,**], L. G. Huey[1], R. Stickel[1], J.Liao[1], M. Shao[2], T. Zhu[2], L. Zeng[2], A. Amoroso[3], F. Costabile[4], C.-C. Chang[5], and S.-C. Liu[5]

[1]School of Earth and Atmospheric Science, Georgia Institute of Technology, Atlanta, GA, USA
[2]College of Environmental Sciences and Engineering, Peking University, Beijing, China
[3]Institute for Atmospheric Pollution, National Research Council (CNR-IIA), Rome, Italy
[4]Institute for Atmospheric Sciences and Climate (ISAC), CNR, Rome, Italy
[5]Research Center for Environmental Changes (RCEC), Academic Sinica, Taipei, China
[*]now at: Combustion Research Facility, Sandia National Laboratories, Livermore, CA, USA
[**]now at: the Pacific Northwest National Laboratory, Richland, Washington, USA

Correspondence to: Z. Liu (zheliu@sandia.gov)

Abstract. We analyze summertime photochemistry near the surface in Beijing, China, using a 1-D photochemical model (Regional chEmical and trAnsport Model, REAM-1D) constrained by in situ observations, focusing on the budgets of RO_x (OH + HO_2 + RO_2) radicals and O_3 formation. While the modeling analysis focuses on near-surface photochemical budgets, the implications for the budget of O_3 in the planetary boundary layer are also discussed. In terms of daytime average, the total RO_x primary production rate near the surface in Beijing is 6.6 ppbv per hour (ppbv h^{-1}, among the highest found in urban atmospheres. The largest primary RO_x source in Beijing is photolysis of oxygenated volatile organic compounds (OVOCs), which produces HO_2 and RO_2 at 2.5 ppbv h^{-1} and 1.7 ppbv h^{-1}, respectively. Photolysis of excess HONO from an unknown heterogeneous source is the predominant primary OH source at 2.2 ppbv h^{-1}, much larger than that of O^1D+H_2O (0.4 ppbv h^{-1}). The largest RO_x sink is via OH + NO_2 reaction (1.6 ppbv h^{-1}), followed by formation of RO_2NO_2 (1.0 ppbv h^{-1}) and $RONO_2$ (0.7 ppbv h^{-1}). Due to the large aerosol surface area, aerosol uptake of HO_2 appears to be another important radical sink, although the estimate of its magnitude is highly variable depending on the uptake coefficient value used. The daytime average O_3 production and loss rates near the surface are 32 ppbv h^{-1} and 6.2 ppbv h^{-1}, respectively. Assuming NO_2 to be the source of excess HONO, the NO_2 to HONO trans-

formation leads to considerable O_3 loss and reduction of its lifetime. Our observation-constrained modeling analysis suggests that oxidation of VOCs (especially aromatics) and heterogeneous reactions (e.g. HONO formation and aerosol uptake HO_2) play potentially critical roles in the primary radical budget and O_3 formation in Beijing. One important ramification is that O_3 production is neither NO_x nor VOC limited, but in a transition regime where reduction of either NO_x or VOCs could result in reduction of O_3 production. The transition regime implies more flexibility in the O_3 control strategies than a binary system of either NO_x or VOC limited regime. The co-benefit of concurrent reduction of both NO_x and VOCs in reducing column O_3 production integrated in the planetary boundary layer is significant. Further research on the spatial extent of the transition regime over the polluted eastern China is critically important for controlling regional O_3 pollution.

1 Introduction

Photochemical smog was first documented in 1950s in Los Angeles (Haagen-Smit and Fox, 1954), and is nowadays a prevalent air pollution phenomenon around the world (e.g., Molina and Molina, 2004; Monks, et al., 2010). A major contributor to smog is the production of secondary pollutants

such as O_3 and aerosols from photochemical reactions involving NO_x ($NO_x \equiv NO + NO_2$) and volatile organic compounds (VOCs), which are emitted from various anthropogenic and natural sources. Over the past decades, continuously improving knowledge of photochemical pollution has successfully served as the basis for formulating the pollution control strategies in the United States (NRC, 1991; NARSTO, 2000). Uncertainties of photochemical modeling in some regions remain large due to the lack of accurate emission inventories (NARSTO, 2005; Liu et al., 2012) and the current incomplete knowledge of chemistry (e.g. Volkamer et al., 2010; Lin et al., 2012).

A region of concern is China. The rapidly increasing emissions of NO_x and VOCs over China since 1980s driven by economic growth have been observed by satellites (e.g., Richter et al., 2005) and documented in bottom-up inventories (e.g., Zhang et al., 2009). As an expected consequence, elevated O_3 (e.g., Wang et al., 2006) and peroxy acetyl nitrates (PANs) (e.g., Liu et al., 2010) accompanied by high loadings of aerosols (e.g. Chan and Yao, 2008; Zhang et al., 2008) have been observed in the country. Severe O_3 and aerosol pollution on an unprecedented large regional scale (Zhao et al., 2009a; van Donkelaar et al., 2010) have also drawn attention given the large impact on public health.

Furthermore, some recent observations over China highlighted the complexity of photochemistry that cannot be fully explained by current knowledge. For example, surprisingly high daytime HONO concentrations from unknown sources have been observed in Beijing (An et al., 2009) and the Pearl River Delta (PRD) region (Su et al., 2008, 2011). At a suburban site in PRD, current standard photochemistry could not explain the observed level of OH, the key oxidant in the troposphere (Hofzumahaus et al., 2009; Lu et al., 2012). Due to the high loading of aerosols, heterogeneous chemistry appears to strongly affect the radical budget (Kanaya et al., 2009) and reactive nitrogen processing (Pathak et al., 2009). A case in point is that we still do not have a clear understanding of how the large emission reductions affected secondary pollutants during the 2008 summer Beijing Olympic and Paralympic Games. The chemical transport modeling study by Yang et al. (2011) demonstrated highly variable chemical sensitivities of O_3 to its precursor emissions due to the uncertain emissions of aromatic VOCs. However, the sensitivity relations are very difficult to derive from observations. For example, Wang et al. (2010) found increases of O_3, sulfate and nitrate while NO_x and VOCs decreased at an urban site in Beijing in the first two weeks after the emission control for the Olympics Game. A similar finding was reported at another urban site in Beijing (Chou et al., 2011). These findings reflect the fact that the effects on O_3 from precursor emission changes can be masked by the variations in the spatial pollutant distribution and meteorological conditions for dispersion, transport, and chemical photolysis.

Given the difficulty of interpreting observations, an alternative approach is through in-depth observation-based modeling analyses to probe into the chemical system. In this work, we analyze the O_3 photochemical processes in Beijing in August 2007 during the CAREBeijing (Campaigns of Air quality REsearch in Beijing) Experiment employing the 1-D version of the Regional chEmical and trAnsport Model (REAM-1D) constrained by observed chemical species and physical parameters, including O_3, NO, PAN, HONO, VOCs, and aerosol surface areas. Through detailed chemical budget analysis, we aim to gain a detailed understanding of the budgets of RO_x (OH + HO_2 + organic peroxy radicals (RO_2)) radicals and formation processes of O_3. A relatively large number of sensitivity experiments are conducted to address the uncertainties in chemistry and diagnose the response of O_3 formation to emission control strategies. The sensitivity experiments are chosen to understand the impacts of aromatics, the observed high concentrations of HONO in daytime, and aerosol uptake of HO_2 separately, such that the effects of the uncertainties in measurements and chemical understanding are apparent from the model results.

The remainder of the paper proceeds as follows. In Sect. 2, we describe the measurement methods and the REAM-1D model (model setup, sensitivity experiments, and diagnostics). Section 3 presents the modeling analysis results. We show the budgets of RO_x radicals in Sect. 3.1, which will also form the basis for analyzing production and loss rates of O_3 in Sect. 3.2. We then further elaborate on the significant roles and uncertainties of aromatics, HONO, and aerosol uptake of HO_2 in the budgets of radicals and O_3, respectively, in Sect. 3.3. The sensitivities of O_3 production to NO_x and VOCs are examined in Sect. 3.4. Finally, in Sect. 4, we summarize our findings and discuss the implications for O_3 pollution control strategies over China.

2 Methodology

2.1 Measurement methods

During the CAREBeijing-2007 experiment (Zhu et al., 2009), a full suite of trace gases were measured concurrently in August 2007 at an urban site located on a building roof top (~20 m above the ground level) on the campus of Peking University (PKU) (39.99° N, 116.31° E). Nitrogen monoxide (NO) was measured with a custom-made chemiluminescence detector (Ryerson et al., 2000). Total reactive nitrogen compounds (NO_y gas-phase only) were measured by the conversion of the NO_y species to NO on a molybdenum converter operated at 300 °C. PAN was measured using a chemical ionization mass spectrometer (CIMS) (Slusher et al., 2004). HONO was measured with a liquid coil scrubbing/UV-VIS instrument (Amoroso et al., 2006). O_3 and CO were measured by commercial instruments from the ECOTECH (EC9810 and EC9830). C_3-C_9 NMHCs were measured with a time resolution of 30 min using two online GC–FID/PID systems (Syntech Spectra

GC–FID/PID GC955 series 600/800 VOC analyzer), one for the C_3–C_5 NMHCs, and the other for C_6-C_9 NMHCs (Shao et al., 2009). Another automated GC/MS/FID system was deployed to measure NMHCs in daytime (08:00–09:00 and 13:00–14:00) (Hofzumahaus et al., 2009). OVOCs were measured using the PFPH–GC/MS method (Ho and Yu, 2004). Size distributions of aerosols (3 nm–10 μm) measured every 10 min with a Twin Differential Mobility Particle Sizer -Aerodynamic Particle Sizer (TDMPS-APS) were used to calculate aerosol surface areas. The uncertainties (1σ) for these measurements are estimated to be 5 % for NO, O_3, CO, 3–5 % for NMHCs, 10 % for NO_y, PAN, HONO and OVOCs. More detailed descriptions of the instruments and measurement methods are available in the supplement.

2.2 The REAM-1D model and sensitivity experiments

The 3-D version of the Regional chEmical and trAnsport Model (REAM-3D) has been applied in a number of studies on O_3 photochemistry and transport at northern mid-latitudes (Choi et al., 2005, 2008a, b; Wang et al., 2007; Zhao et al., 2009a, b, 2010; Zhao and Wang, 2009; Yang et al., 2011; Liu et al., 2012). The REAM-1D model shares the modules for O_3-NO_x-hydrocarbon photochemistry, vertical diffusion, convective transport, and wet/dry deposition (Liu et al., 2010) with the REAM-3D model. The chemical kinetics data were updated with the latest compilation by Sander et al. (2011), and the VOC chemistry in REAM-3D is expanded to include the chemistry of aromatics based on the SAPRC-07 chemical mechanism (Carter, 2009). Vertical transport is driven by WRF assimilated meteorological fields based on the NCEP reanalysis data (Zhao et al., 2009a). Meteorological parameters (i.e. water vapor concentrations, temperature, pressure, and diffusion coefficient) in the model are taken from WRF outputs. Photolysis rates are dependent on cloud fraction and optical depth calculated based on WRF meteorological fields (Choi et al., 2008b).

The standard 1-D model is constrained with measured CO, O_3, NO, HONO, NMHCs (C_2–C_9), OVOCs (acetone, acetaldehyde and formaldehyde) and aerosol surface areas in the first layer. With these tracers transported vertically (mostly via eddy diffusion), such a setup is similar to a 1-D model with specified emissions from the surface (Trainer et al., 1991), except that the model in this study is constrained by available observations. 3-D REAM model simulated chemical tracer concentrations (Zhao et al., 2010) in the column over Beijing were used as initial and boundary conditions at upper model layers. For measurements made with a time resolution longer than 1 min (e.g. NMHCs and OVOCs, aerosol surface areas), constant measured values were assigned during the measurement period. Missing data points on some days due to instrumental issues were replaced with the corresponding value in the overall average diurnal profile at the time of missing data. The 1-D model was run with a 1-min time step, continuously from 1 August to 30 August

2007 and the results for the last 20 days were analyzed after a spin-up time of 10 days. The REAM-1D model with such a setup is able to reproduce the observed PAN near the surface in Beijing, which has been shown to have equal contributions by chemistry near the surface and from downward vertical transport (Liu et al., 2010). In addition to resolving vertical mixing in the planetary boundary layer (PBL), the 1-D model allows for explicit computation of dry deposition rates, which are assumed or estimated as lifetime parameters in box models. For additional information of the REAM-1D model and its performance, we refer the readers to the supplement and Liu et al. (2010).

OVOC and HONO both have photochemical sources and sinks. Their concentrations in the model cannot be specified using observed values when the sensitivities of RO_x budgets and O_3 production to these species are analyzed. Model simulated OVOCs, including formaldehyde, acetaldehyde, and acetone, methylglyoxal, and glyoxal, agree with the observations within 20 % in terms of daytime average concentrations (Table S3 in the Supplement), indicating that secondary production is their predominant source. Removing the constraint of observed OVOCs in the standard model did not lead to notable changes in the simulated RO_x concentrations or O_3 production/loss rates. Exceptionally high levels of HONO were observed at daytime ($\sim$1 ppbv in the afternoon) during the study period. The gas-phase source from the NO+OH reaction alone could only explain a minor portion ($\sim$10 %) of the observed HONO concentrations. In order to investigate the photochemical impact of this missing source of HONO, we introduce a pseudo-reaction of $NO_2 \rightarrow HONO$ in the model (at a rate of 6.4×10^{-5} s^{-1} on average during daytime, in the first model layer near the surface) to reproduce the observed daytime HONO and quantitatively estimate the primary radical source from the heterogeneous HONO production pathway. Replacing the observed HONO with the pseudo HONO production does not lead to notable changes in RO_x concentrations.

Due to the large aerosol surface areas ($\sim$1000 μm^{-2} cm^{-3}), the uptake of HO_2 by aerosols may become a large HO_2 sink. The HO_2 aerosol reactive uptake coefficient, γ, is still quite uncertain and may be a function of temperature and aerosol composition (Thornton and Abbatt, 2005; Thornton et al., 2008; Kanaya et al., 2009; Mao et al., 2010). In this work, we chose a moderate value of γ (HO_2) = 0.02 in the standard model (S0 in Table 1) (Thornton et al., 2008), and we evaluate model sensitivities by varying the value of γ (HO_2) from 0 to 0.2, a range covering the general range of γ (HO_2) (e.g., Thornton et al., 2008).

Besides the standard model S0, we designed and conducted a number of sensitivity simulations summarized in Table 1. S0 is the standard model, while S0a and S0b are S0 with varied γ (HO_2) values, 0 in S0a and 0.2 in S0b, respectively. S1 is S0 without the "excess" HONO that cannot be explained by gas-phase HONO production; S2 is S0 without

Table 1. Sensitivity simulation scenarios.

Scenarios or purposes	Description
S0	Standard model setup: with full VOC chemistry, excess HONO, γ (HO$_2$) = 0.02
S0a	S0 with γ (HO$_2$) = 0
S0b	S0 with γ (HO$_2$) = 0.2
S1	S0 without excess HONO
S2	S0 without aromatics
S3	S0 without excess HONO or aromatics
S3a	S3 with γ (HO$_2$) = 0
P(O$_3$)$_{senst}$	S0, S0b, S1, S2, S3, S3a constrained with 50 %, 70 %, 90 %, 110 % of observed values of NO, VOCs respectively, and both of them
γ (HO$_2$)$_{senst}$	S0 with γ (HO$_2$) = 0, 0.02, 0.05, 0.1, 0.15, 0.2

aromatics; S3 is S0 without excess HONO or aromatics, and S3a further removes the aerosol HO$_2$ uptake (γ (HO$_2$) = 0) in S3. These experiments (S1–S3, γ (HO$_2$)$_{senst}$) further examine the sensitivities of radical budgets and O$_3$ production to those key factors identified in S0, including aromatic VOCs, daytime HONO concentrations, and aerosol uptake of HO$_2$, which have considerable uncertainties due to the current incomplete knowledge in the related processes (Sect. 3.3). The P(O$_3$)$_{senst}$ simulations compare O$_3$ production rates under varied NO$_x$ and VOCs conditions. In these sensitivity simulations, we did not constrain HONO or OVOCs to the observations in order to retain the feedback from them.

2.3 Model diagnostics

The 1-D modeling is constrained by surface observations. Vertical profiles of O$_3$ and its precursors are also simulated by turbulence transport from the surface. We can diagnose the radical and O$_3$ budgets near the surface and in the PBL. We focus the model diagnostics on the budgets near the surface for two reasons. Ozone and its precursors are simulated in the PBL and are specified to the observations near the surface. The near-the-surface model diagnostics are therefore less uncertain than in the PBL. Heterogeneous processes of excess HONO production and aerosol uptake of HO$_2$ are only simulated near the surface since we only have the observed HONO and aerosol size distribution near the surface. The radical budgets cannot be properly analyzed in the PBL given the importance of these heterogeneous processes. We will, however, present the O$_3$ budget analysis in the PBL. The concentrations of O$_3$ near the surface are affected by the production rates in the PBL because of the relatively long chemical lifetime of O$_3$. The integration of O$_3$ budget terms is described in the supplement. In the following sections, all the PBL analysis results are specifically noted. If not noted, the analysis is for the surface layer.

3 Results and discussions

O$_3$ formation and the chemical dependence on the emissions of O$_3$ precursors involve production and recycling of a variety of RO$_x$ radicals. In this section, we first present the abundance and budgets of RO$_x$ radicals calculated with the observation-constrained 1-D model, to identify the main features and uncertainties of photochemistry in Beijing. By focusing on the chemical pathways controlling O$_3$ production and loss, and their responses to varied precursors, we then quantify the rates of O$_3$ formation and diagnose its chemical regime.

3.1 Budgets of RO$_x$ radicals

3.1.1 Model simulated concentrations of OH, HO$_2$ and RO$_2$

Figure 1 shows the average diurnal profiles of OH, HO$_2$ and RO$_2$ concentrations simulated in the standard model (S0). The 20-day average diurnal maximum concentrations of OH, HO$_2$, and RO$_2$ are 9×10^6, 6.8×10^8, and 4.5×10^8 molecules cm^{-3}, respectively. RO$_x$ radical measurements over mainland China are still sparse. To put our simulated concentrations in context, the simulated maximum OH concentration (9×10^6 molecules cm^{-3}) in this study for Beijing is ∼50 % higher than that simulated over Mountain Tai in June of 2006 (6×10^6 molecules cm^{-3}) (Kanaya et al., 2009), and lies between the observed (13×10^6 molecules cm^{-3}) and simulated (7×10^6 molecules cm^{-3}) values at a site in PRD (Hofzumahaus et al., 2009). The maximum HO$_2$ concentration simulated for Beijing (6.8×10^8 molecules cm^{-3}) is close to that over Mountain Tai (Kanaya et al., 2009), and is only half of that in PRD (Hofzumahaus et al., 2009). We note that HO$_2$ concentrations simulated over China (Kanaya et al., 2009 and this work) are quite sensitive to γ (HO$_2$), due to the large abundance of aerosols. Interestingly, removing the aerosol HO$_2$ sink in this study would lead to higher simulated HO$_2$ and OH concentrations that are in good agreement with the observed values at the PRD site by Hofzumahaus et al. (2009), although the locations and time of the two studies are different. Compared to urban areas outside China, the simulated OH and HO$_2$ concentrations for Beijing are similar to those observed in Mexico City (Shirley et al., 2006; Dusanter et al., 2009), and yet higher than those in New York City (Ren et al., 2003) and Birmingham of the UK (Emmerson et al., 2005a).

RO$_2$ radicals include all organic peroxy radicals derived from VOC oxidation, and are categorized into 7 groups (Fig. 1), i.e. methyl peroxy radicals (CH$_3$O$_2$), first generation peroxy radicals from alkanes (ALKA$_p$), alkenes except isoprene (ALKE$_p$), isoprene (ISO$_p$), aromatics (ARO$_p$), acyl peroxy radicals (RCO$_3$), and peroxy radicals from OVOCs (OVOC$_p$). The three most abundant groups of RO$_2$
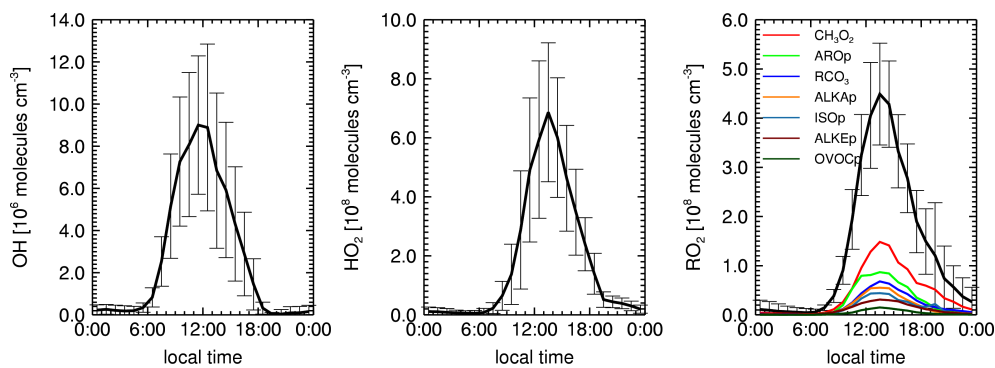
Fig. 1. Average diurnal profiles of OH, HO_2 and RO_2 (black lines) in the standard model (S0). The vertical bars show the hourly standard deviations. The color lines in the rightmost panel show the major components of RO_2, which are described in the text.
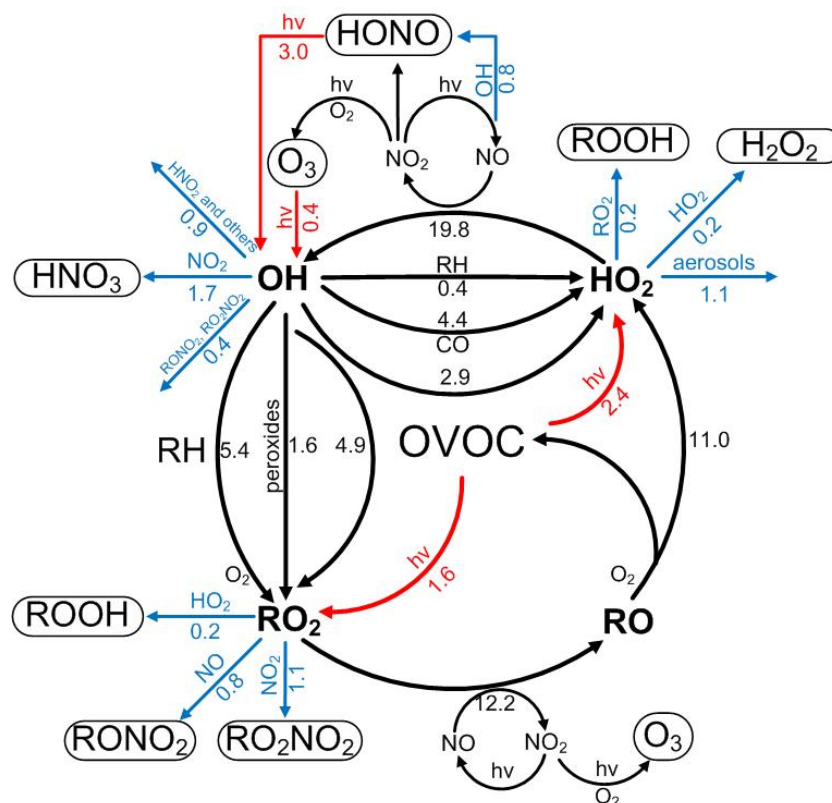

Fig. 2. Daytime (06:00–18:00) average budgets of RO_x radicals. Primary RO_x sources and sinks are in red and blue, respectively. The production and loss rates are in ppbv h^{-1}.

are CH_3O_2, AROp and RCO_3. CH_3O_2 makes the largest contribution as expected. Aromatics have higher concentrations and OH reactivities than alkenes and alkanes (Liu et al., 2010), producing more RO_2 radicals upon oxidation. $RC(O)O_2$ radicals are produced from OH oxidation or photolysis of a variety of carbonyl compounds. $CH_3C(O)O_2$ is the simplest and most abundant $RC(O)O_2$, and also the precursor of PAN. Liu et al. (2010) showed that methylglyoxal from aromatics is the predominant source ($\sim$75 %) of $CH_3C(O)O_2$ and PAN in Beijing.

3.1.2 RO_x budgets

Figure 2 illustrates schematically the RO_x daytime (06:00–18:00) budgets simulated in the model. Minor RO_x radical sources (<0.1 ppbv h^{-1}), e.g. ozonelysis of alkenes, are not shown. The reactions of NO + HO_2 (19.8 ppbv h^{-1}) and NO + RO_2 (12.2 ppbv h^{-1}) are the two largest pathways of radical cycling in the system, mainly due to the abundance of NO (e.g. $\sim$ 5 ppbv around noontime). As a result, the fast RO_x cycling is mainly driven by these two NO + RO_x reactions, as
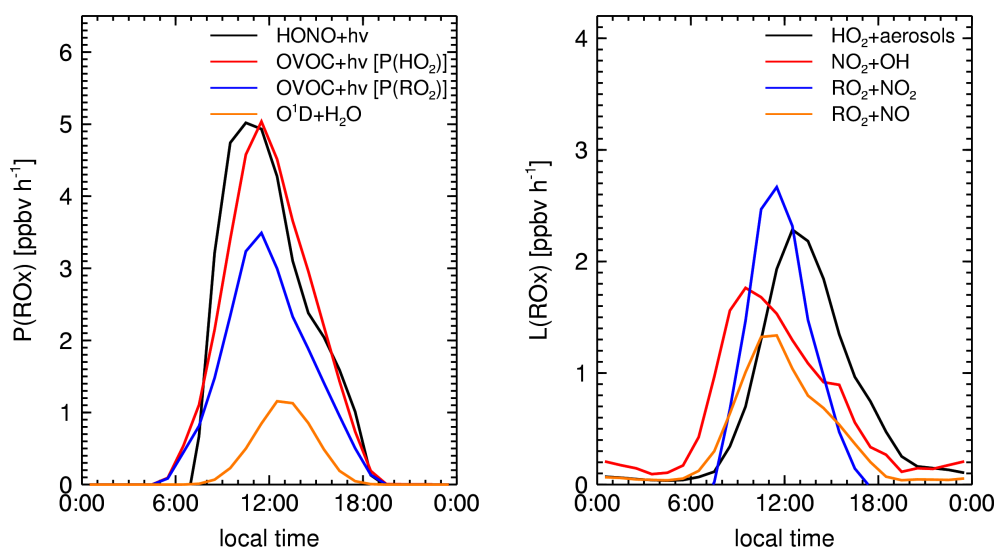
Fig. 3. Average diurnal profiles of major RO_x primary sources and sinks.

typically seen in NO_x-rich environments (Emmerson et al., 2005b; Shirley et al., 2006; Dusanter et al., 2009; Elshorbany et al., 2009).

Besides the efficient radical cycling, the primary sources and sinks of radicals are also very large in Beijing. Photolysis of OVOCs turns out to be the predominant primary RO_x source (4.0 ppbv h^{-1}), and also the largest sources of HO_2 (2.4 ppbv h^{-1}) and RO_2 (1.6 ppbv h^{-1}), consistent with previous urban studies (Jenkin et al., 2000; Emmerson et al., 2005b; Dusanter et al., 2009). Photolysis of excess HONO is the second largest RO_x source (3.0−0.8 = 2.2 (ppbv h^{-1})), as well as the largest source of OH. At noontime the excess HONO produces OH at ∼5 ppbv h^{-1} (Fig. 3), a rate that is comparable to that found by Su et al. (2008) at Xinken in PRD, and slightly higher than that at another site, Backgarden, in the same region (Hofzumahaus et al. 2009). By contrast, the reaction of O^1D + H_2O only contributes 0.4 ppbv h^{-1} of the primary OH production, less than 1/5 of the excess HONO source, which is consistent with the finding in PRD by Hofzumahaus et al. (2009). It should be noted that these aforementioned excess daytime HONO sources inferred over China are significantly larger than most urban areas outside China (e.g. Acker et al., 2006; Kleffmann, 2007 and references therein; Dusanter et al., 2009; Elshorbany et al., 2009; Costabile et al., 2010). Summing up all these aforementioned sources gives a total primary RO_x production rate at 6.6 ppbv h^{-1} (2.6 ppbv h^{-1} for OH, 2.4 ppbv h^{-1} for HO_2, and 1.6 ppbv h^{-1} for RO_2), which is comparable to that in Santiago, Chile (7.0 ppbv h^{-1}) (Elshorbany et al., 2009), but ∼50 % higher than those in Mexico City in 2006 (4.75 ppbv h^{-1}) (Dusanter et al., 2009), and Birmingham of the UK (4.5 ppbv h^{-1}) (Emmerson et al., 2005b).

RO_x radicals are ultimately removed from the atmosphere via deposition of radical reservoir species, e.g. HNO_3, H_2O_2,

ROOH. The net radical losses via NO_x-radical reactions are 3.6 ppbv h^{-1}, including NO_2 + OH producing HNO_3 (1.7 ppbv h^{-1}), RO_2 + NO_2 producing organic peroxy nitrates (RO_2NO_2, mostly PANs) (1.1 ppbv $^{-1}$), and RO_2 + NO producing organic nitrates ($RONO_2$) (0.8 ppbv h^{-1}). By contrast, the radical loss rates via radical-radical reactions producing peroxides such as H_2O_2 and ROOH are much lower (0.6 ppbv h^{-1} in total). Such a contrast has been typically seen as a feature of chemistry in NO_x-rich urban environments. Another important and still uncertain RO_x sink in Figs. 2 and 3 is the aerosol uptake of HO_2 (1.1 ppbv h^{-1}), mainly owing to the abundant aerosols in Beijing. The magnitude of this radical sink varies significantly with values of γ (HO_2) used in the model (Sect. 3.3.3). It is also noteworthy that the two RO_2 + NO_x reaction pathways collectively contribute a net RO_x loss at 1.9 ppbv h^{-1}, larger than that of NO_2+OH (1.6 ppbv h^{-1}), which is different from most urban environments outside China (Emmerson et al., 2005b; Dusanter et al., 2009; Elshorbany et al., 2009). Figure 4 shows the diurnal transition of RO_2NO_2 production and loss. During most of the daytime, RO_2NO_2 production dominates over its loss processes (mainly via thermal decomposition) leading to the net formation of RO_2NO_2 and thus sequestering of NO_2 and $R(O)O_2$ radicals. RO_2NO_2 loss starts to dominate over production from late afternoon into evening. Such a diurnal transition of RO_2NO_2 production and loss differs from the often used steady-state assumption of RO_2NO_2, and has considerable impacts on O_3 production (Sect. 3.2). $RONO_2$ is formed from minor channels in NO + RO_2 reactions, and the importance of these channels is known to be a function of the size of RO_2. $RONO_2$ has longer lifetimes (at least 2 days) than RO_2NO_2, and its loss by transport and deposition is a net loss of RO_x radicals.
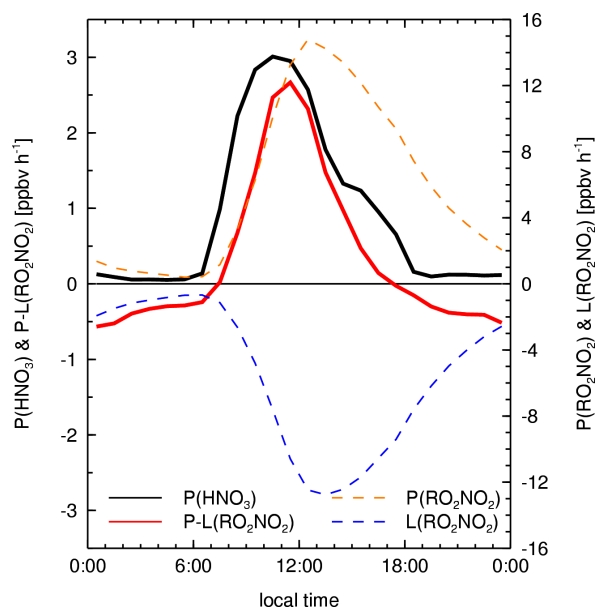
Fig. 4. Average diurnal profiles of net formation rates of RO_2NO_2 and HNO_3. Production and loss rates of RO_2NO_2 are also shown.

Another feature of the chemical system in Fig. 2 is the coupling of NO_x and VOCs chemistry and the comparable importance of their roles as RO_x sources and sinks. Both NO_x and VOCs affect major RO_x primary sources, i.e. the source OH from excess HONO ($2.2\,ppbv\,h^{-1}$) and photolysis of OVOCs ($4.2\,ppbv\,h^{-1}$). Both of them affect RO_x sinks through organic nitrates. This feature of chemistry could have implications for O_3 sensitivities to NO_x and VOCs (Farmer et al., 2011). In Section 3.2 – 3.3, we examine the formation of O_3, and its sensitivities to various factors, including excess HONO, aromatics, γ (HO_2), as well as NO_x and VOCs.

3.2 O_3 photochemistry

3.2.1 O_3 production and loss rates

The formation of O_3 in the troposphere is via the reactions of NO and peroxy radicals. On the other hand, due to the fast cycling of both O_3 and NO_2 under urban conditions, O_3 loss is due to a number of reactions leading to the destruction of O_3 and NO_2. The daytime average $P(O_3)$ is the sum of $HO_2 + NO$ ($19.8\,ppbv\,h^{-1}$) and $RO_2 + NO$ ($12.2\,ppbv\,h^{-1}$) at $32\,ppbv\,h^{-1}$ (Fig. 2), comparable to previous calculations for Beijing during CAREBeijing-2006 (Lu et al., 2012), and is near the top of the existing reported values for urban environments (e.g. Ren et al., 2003; Shirley et al., 2006; Kanaya et al., 2008; Wood et al., 2009). The reaction of $HO_2 + NO$ accounts for roughly 2/3 of $P(O_3)$. $RCO_3 + NO$, $CH_3O_2 + NO$ and $AROp + NO$ are the predominant $RO_2 + NO$ reactions, due to the relative abundance of RO_2 radicals (Fig. 1) and the large reaction rate constant of $RCO_3 + NO$. The mean

daytime peak of $P(O_3)$ is $\sim 60\,ppbv\,h^{-1}$, occurring around 11:00 (Fig. 5), earlier than the peaks of both HO_2 and RO_2 around 13:00 because of the decreased NO concentrations from morning to early afternoon. $P(O_3)$ is also found to peak around 10:00–11:00 local time in Mexico City (Shirley et al., 2006). The corresponding PBL averaged O_3 production and net formation rates are shown in Fig. S1 of the Supplement. The rates are about a factor of 4 lower reflecting the simulated decrease of theese rates with altitude (Fig. S2 in the Supplement).

The daytime mean and maximum $L(O_3)$ rates are $6.2\,ppbv\,h^{-1}$ and $12\,ppbv\,h^{-1}$, respectively, roughly 1/5 of $P(O_3)$. $L(O_3)$ consists of $NO_2 \rightarrow$ HONO ($2.2\,ppbv\,h^{-1}$), $NO_2 + OH$ ($1.7\,ppbv\,h^{-1}$), $RO_2 + NO_2$ ($1.1\,ppbv\,h^{-1}$), $O^1D + H_2O$ ($0.4\,ppbv\,h^{-1}$), and other minor reactions. Given the noontime O_3 and NO_2 concentrations ($\sim 55\,ppbv$ and $\sim 10\,ppbv$) and the loss rate of O_3, the chemical lifetime of O_3 is $\sim 5\,h$. It is interesting that the unknown source of HONO (assuming NO_2 to be the precursor) also serves as a $L(O_3)$ term, and is in fact the largest $L(O_3)$ reaction ($\sim 40\%$), directly affecting O_3 formation and the lifetime of O_3. Such a potential O_3 loss process associated with HONO is worth further investigation. The average daytime net formation rate of O_3, i.e. $P(O_3) - L(O_3)$, is $\sim 26\,ppbv\,h^{-1}$.

Rapid surface O_3 formation at a similar rate in Beijing and its vicinity were also reported previously (Lou et al., 2010). However, it should be noted that the O_3 formation rate near the surface is one of many factors affecting surface O_3 concentrations (e.g., Shirley et al., 2006). Inspection of the model results shows a decrease of O_3 production rates with altitude (Fig. S2 in the Supplement) due largely to a corresponding decrease in NO concentrations. When averaged over the whole PBL, the daytime average gross and net O_3 production rates of $6.7\,ppbv\,h^{-1}$ and $5.0\,ppbv\,h^{-1}$, respectively, are much slower than those near the surface (Figs. S1 and S3 in the Supplement). Our results point to the importance of obtaining the vertical profiles of O_3 precursors in the PBL in order to better constrain model simulations and improve the understanding of factors controlling O_3 concentrations near the surface. While the vertical turbulent transport and surface dry deposition are taken into account in the 1-D model, horizontal advection also plays an important role. Although the 1-D model cannot be used in predicting surface O_3 concentrations, the increase of O_3 concentrations in daytime due to the net production in the PBL is reflected in the surface O_3 observations (Liu et al., 2010).

3.2.2 O_3 production efficiency

Alongside O_3 formation, NO_x is transformed into oxidized nitrogen compounds NO_z ($NO_z \equiv NO_y - NO_x$), e.g. $RONO_2$, RO_2NO_2, and HNO_3, and then eventually removed from the atmosphere by deposition. NO_z compounds at daytime account for 20–50 % of total NO_y (Fig. 6). The O_3 production efficiency (OPE) of NO_x is defined as the amount of O_3
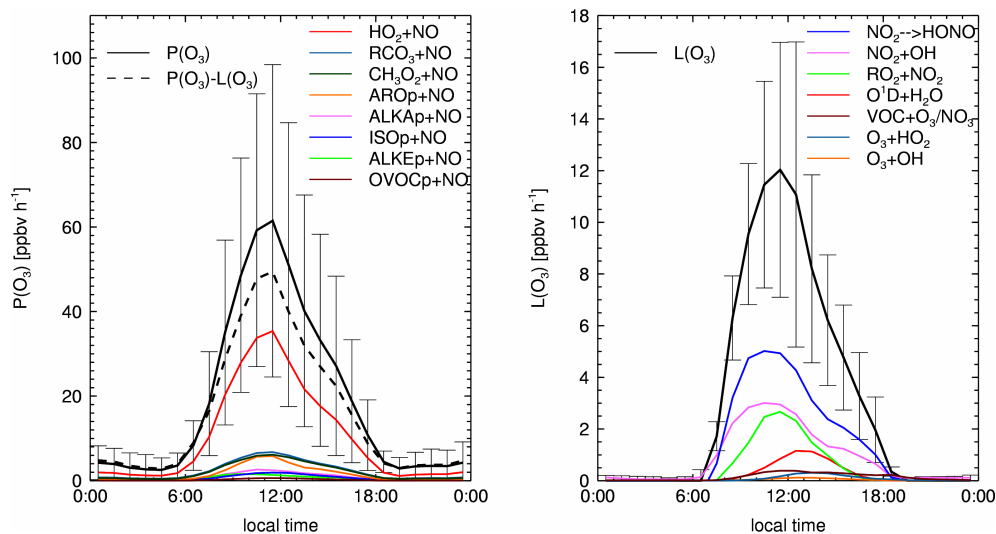
Fig. 5. Average diurnal profiles and breakdowns of O$_3$ production (left) and loss rates (ppbv h^{-1}) (right). The vertical bars show the standard deviation.
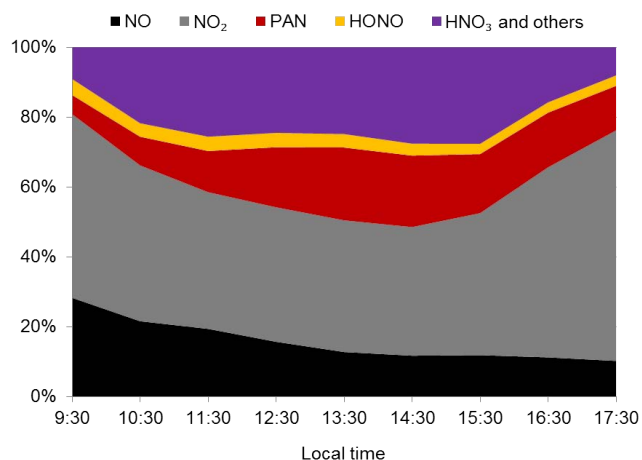

Fig. 6. Daytime evolution of NO$_y$ components.

produced during the lifetime of NO$_x$ (Liu et al., 1987). Based on our model calculated P(O$_3$) and P(NOz) (Fig. 2), we estimate a daytime average OPE to be 9.7, much larger than that estimated by Wang et al. (2010) for the summer of 2008, and yet within the estimates by Chou et al. (2011) for the summer of 2006. It is also within the estimated range for Mexico City (4–12) (Lei et al., 2007; Wood et al., 2009). Considering the moderate concentrations of HO$_2$ and RO$_2$ compared to other urban environments, the relatively high OPE from our calculation is mainly due to the high daytime NO concentration ($\sim$5 ppbv at noontime). When averaged over the whole PBL, the OPE value of 11.7 is higher than estimated near the surface.

3.3 Sensitivity studies – assessing the impacts of HONO, aromatics and aerosol uptake of HO$_2$

Based on the results from the standard model (S0) results discussed above, we found that excess HONO, reactive aromatic VOCs, and aerosol uptake of HO$_2$ are important factors in the photochemical system in Beijing. In the next section, in order to further address the uncertainties in these factors, we extend our analyses of these individual factors by comparing results from a series of sensitivity simulations listed in Table 1.

3.3.1 Impacts of excess HONO on RO$_x$ budgets and O$_3$ formation

The large net OH source from the photolysis of excess HONO relative to other primary OH sources has been shown in Fig. 2. Figure 7 shows the sensitivity simulation results without excess HONO (S1). The standard model (S0) has $\sim$60 % higher daytime average OH concentration than S1 due to the excess HONO. Increased OH leads to more active photochemistry and thus $\sim$50 % increases of HO$_2$ and RO$_2$ concentrations, as well as P(O$_3$). A similar amplifying effect by HONO on P(O$_3$) was also noted by Lou et al. (2010). A second consequence is the large sink ($\sim$40 %) of O$_3$ due to excess HONO production (Section 3.2). The impact of excessive HONO is even larger ($\sim$130 %) when aromatics are not included (comparing Figs. S3 to S2 in Fig. 7). This excess HONO term is usually not considered in the budget of O$_3$ in previous studies. For locations like Beijing, it appears necessary to take into account the production and loss of O$_3$ due to excess HONO. More importantly, the nature of excess HONO is currently unknown and needs to be considered as a major source of uncertainty for understanding O$_3$.
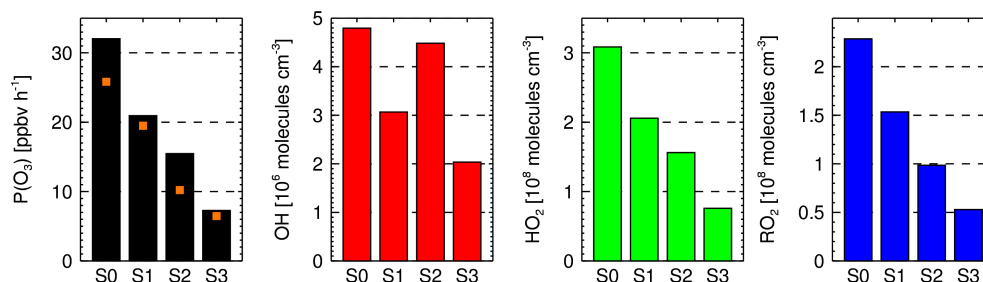
Fig. 7. Daytime average O_3 production rates and concentrations of OH, HO_2, and RO_2 under scenarios S0, S1, S2, and S3. The yellow squares show the net O_3 formation rates ($P(O_3) - L(O_3)$).
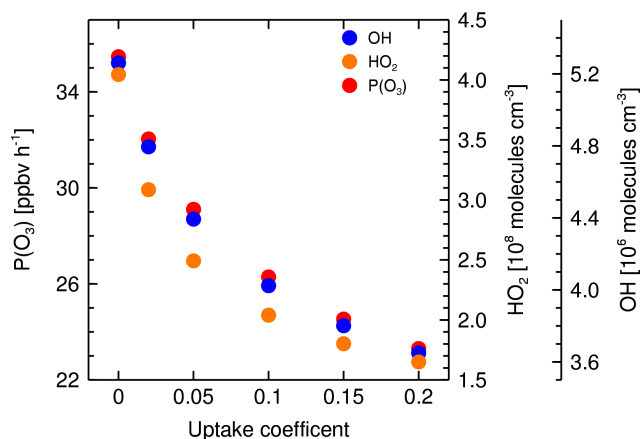

Fig. 8. Daytime average HO_2, OH and $P(O_3)$ as a function of γ (HO_2).

We note that the daytime HONO concentrations measured in this and other studies over China, i.e. roughly 1 ppbv on average during daytime, and the inferred excess HONO formation rates (e.g. Su et al., 2008, 2011; Hofzumahaus et al., 2009; and this work), are substantially higher than those found elsewhere. Although known interference was tested and removed (the Supplement), unknown interference was possible (e.g. Pinto et al., 2010). A well-designed intercomparison with other instruments (such as a long-path differential optical absorption spectroscopy (DOAS) instrument) in Beijing would be necessary. The detailed photochemical analysis presented here by comparing the relative importance of the primary HO_x sources (e.g., Fig. 2) would provide a quantitative assessment on the impact of a potential HONO interference on the O_3 and radical photochemistry if the interference were quantified. We also note that the excess HONO source was only included in the surface layer of the model since the nature of the heterogeneous reaction is not well characterized. Extending this source into the PBL would further increase its impact.

3.3.2 Direct and secondary impacts from aromatics

Aromatics are the most reactive and abundant VOC group measured in Beijing (Liu et al., 2010). The direct impact of aromatics on radical budgets and O_3 formation is via contributing first generation RO_2 (AROp) upon oxidation by OH; and we refer the effect due to subsequent oxidation products as secondary. Comparing S0 with S2 (Fig. 7), adding aromatics leads to a factor of 2 increase of HO_2, RO_2, and $P(O_3)$. These changes obviously could not be explained solely by the addition of AROp radicals (Fig. 5). Inspection of the model results shows that OVOCs concentrations increase drastically after adding aromatics (e.g. ~100 % increase of formaldehyde; ~65 % increase of acetaldehyde, a factor of 5 increase of methylglyoxal and a factor of 10 increase of glyoxal (Table S3 in the supplement)), and their photolysis further produces substantial amounts of primary RO_2 and HO_2. More significantly, the presence of aromatics in S0 increases OH by ~30 % compared to S2 despite of the loss of OH by reacting with aromatics. Therefore, the overall increase of primary RO_x production from the secondary impact by aromatics is large enough to compensate for the shift from OH to peroxy radicals in the RO_x family. If the reactions of excess HONO are not included, the impacts by aromatics (from Figs. S3 to S1) are even more drastic, leading to more than 100 % increase of HO_2, RO_2 and $P(O_3)$, and 50 % increase of OH. We note that the finding on the significance of aromatic VOCs on photochemistry is qualitatively robust. However, the quantitative results presented here depend on the chemical mechanism used for aromatic VOC oxidation, for example, the yields of dicarbonyls, which are uncertain (e.g. Carter, 2009). In situ measurements of OVOC species, especially those dicarbonyls, such as methylglyoxal and glyoxal, will be needed to further constrain the model. When integrated in the PBL, the effect of aromatics is smaller (~25 % by comparing case S0 to S2 in Fig. S3 of the Supplement).

3.3.3 Aerosol uptake of HO_2

Figure 8 shows the variations of daytime average HO_2, OH concentrations and $P(O_3)$ rates as a function of γ (HO_2) value. HO_2 concentration drops by

60 % from 4.05×10^8 molecules cm^{-3} at γ (HO$_2$) = 0 to 1.65×10^8 molecules cm^{-3} at γ (HO$_2$) = 0.2. Correspondingly, P(O$_3$) decreases by $\sim$50 % from 35.4 ppbv h^{-1} to 23.3 ppbv h^{-1}, and OH drops by 30 % from 5.26×10^6 molecules cm^{-3} to 3.65×10^6 molecules cm^{-3}. P(O$_3$) and OH changes are not as large as HO$_2$ in part because the impact of γ (HO$_2$) on RO$_2$ radicals is indirect and not as large. Figure 8 suggests that γ (HO$_2$) is a large source of uncertainty in current HO$_x$ simulation studies over polluted regions of China, where aerosol loading is high (Kanaya et al., 2009). Recently, Taketani et al. (2012) measured ambient γ (HO$_2$) in the range of 0.09 $\sim$ 0.4 over Mt. Mang (40 km north of Beijing), and in the range of 0.13 $\sim$ 0.34 at a remote site over Mt. Tai in China. These γ (HO$_2$) values for ambient aerosols are considerably larger than those estimated by Thornton et al. (2008) or the experimental values for non-metal aerosols compiled by Mao et al. (2012). Additional independent measurements are needed to confirm these high γ (HO$_2$) values over China. Increasing the γ (HO$_2$) value from 0.02 as we assumed to 0.2 would make aerosol uptake of HO$_2$ the predominant primary RO$_x$ sink (Fig. 2) and decrease HO$_2$, OH, and O$_3$ production by 48 %, 24 %, and 28 % (Fig. 8), respectively.

3.4 Chemical regimes of O$_3$ production

We diagnose the P(O$_3$) chemical regimes in Beijing using two approaches. First, we examine the sensitivity of P(O$_3$) to perturbations of NO$_x$ and VOC concentrations. We also try to use previously proposed diagnostic equations (e.g. Sillman et al., 1990; Kleinman et al., 1997; Daum et al., 2000) for NO$_x$-limited and VOC-limited regimes, as has been done in previous studies (Lei et al., 2007). The chemical environment in Beijing is strongly affected by various factors, e.g. excess HONO, aromatics, and aerosol uptake of HO$_2$. These factors are not present in the US where those previous theoretical studies (e.g. Sillman et al., 1990; Kleinman et al., 1997) were conducted. We analyze each scenario listed in Table 1 and then discuss the possible impacts from those factors on P(O$_3$) chemical regimes in Beijing.

3.4.1 Sensitivity simulation results

In the sensitivity analyses (Table 1), we vary NO$_x$ and VOCs concentrations (110 %, 90 %, 70 %, and 50 % of the observed values) and examine the change of P(O$_3$), i.e. ΔP(O$_3$). While it is desirable to study the direct change of O$_3$ due to precursor changes, a box or 1-D model cannot adequately simulate O$_3$ concentrations due to the large impact of advection as noted previously. We therefore diagnose the change of P(O$_3$). The sensitivity results are numerically accurate only when the change of the model state is small. We included large changes (50 % and 70 % reductions) in order to infer the impact of precursor changes on O$_3$ photochemical production

regime. These results represent a linear extrapolation of the sensitivities in the photochemical system.

Figure 9 shows the sensitivity experiment results. P(O$_3$) consistently shows positive responses to ΔNO$_x$, i.e. an increase of NO$_x$ leads to an increase of P(O$_3$), although the former is always larger than the latter, i.e., the ΔP(O$_3$) $-$ ΔNO$_x$ lines are to the left of the 1:1 line. P(O$_3$) is largely determined by the product of NO and HO$_2$ (RO$_2$) concentrations (Fig. 9a). The non-linear dependence of P(O$_3$) on NO$_x$ is a reflection of the dependence of HO$_2$ and RO$_2$ on NO$_x$. For example, increasing NO$_x$ leads to decreased peroxy radicals due in part to the conversion of peroxy radicals to OH and RO by reacting with NO. The degree of peroxy radical decrease is also a function of the change in primary RO$_x$ sources and sinks. Comparing the scenarios without aromatics and HONO (S3 and S3a) with those with both or either one of them (S0, S1 or S2), P(O$_3$) in the former scenarios (S3 and S3a) is much less sensitive to ΔNO$_x$ (e.g., the flat shapes of the orange lines in Fig. 9a). The larger sensitivity of peroxy radicals to NO$_x$ change in S3 and S3a is because of a much smaller primary RO$_x$ source without excess HONO, aromatics or both (Sect. 3.3). Similarly, inspection of the difference between S0 and S0a or among S3, S3a and S3b shows that a larger HO$_2$ aerosol sink leads to a lesser sensitivity of peroxy radicals to NO$_x$ and hence a higher sensitivity of P(O$_3$) to NO$_x$.

The complexity of the P(O$_3$)-NO$_x$ sensitivity also results in part from the change over the course of a day (Fig. 10). Generally, P(O$_3$) shows a larger sensitivity to NO$_x$ in the afternoon than in the morning. Under different scenarios, such as S0 and S3a in Fig. 10, P(O$_3$)-NO$_x$ sensitivities show different transition patterns over the course of daytime. This daytime transition of P(O$_3$)-NO$_x$ sensitivity is due to the fast decreasing NO$_x$ from morning towards afternoon and thus reducing the importance of NO$_x$ in sequestering radicals, while the primary RO$_x$ source increases into the afternoon.

In contrast to the largely varying degrees of sensitivities of P(O$_3$) to NO$_x$, the sensitivity of PO$_3$ to VOCs is much more uniform and closer to the 1:1 linear response (Fig. 9b). The largest deviation from the 1:1 response line is the simulation without aromatics (S2) due to the large impact of aromatics to primary RO$_x$ sources (Sect. 3.3.2). Figure 9a and 9b show that the P(O$_3$)-VOC response resembles the VOC-limited chemical regime (Sillman et al., 1990), although the P(O$_3$)-NO$_x$ response does not, suggesting that photochemical O$_3$ production in Beijing is neither NO$_x$-limited nor VOC-limited, but lies in a transition regime where reduction of either can reduce P(O$_3$).

Concurrent reduction of NO$_x$ and VOC concentrations leads to greater P(O$_3$) reduction than reducing either (Fig. 9c), although the additional reduction from VOC-reduction only scenarios (Fig. 9d) varies. In agreement with the P(O$_3$)-NO$_x$ sensitivity (Fig. 9a), the least change from the VOC-only scenarios is from the simulations S3 and S3a in which neither excess HONO nor aromatics is included.
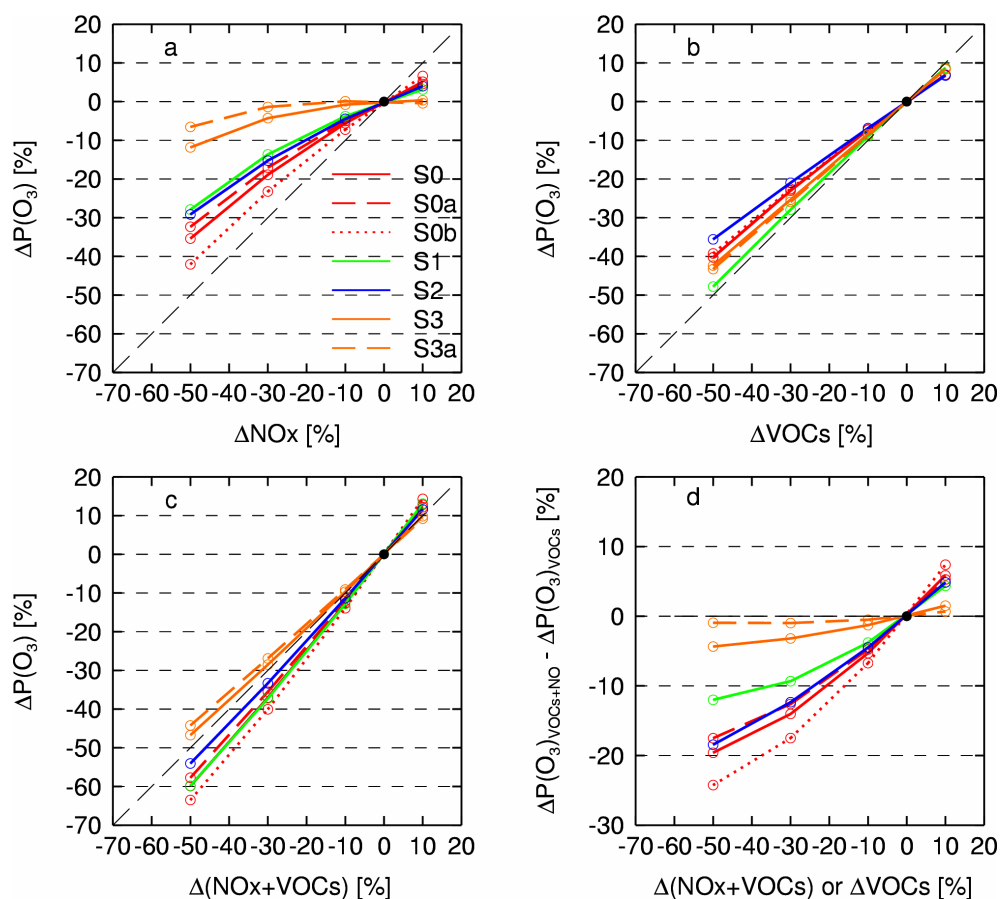
Fig. 9. Changes of O_3 production ($\Delta P(O_3)$) as a function of NO_x, VOCs, and both under different scenarios in Table 1.
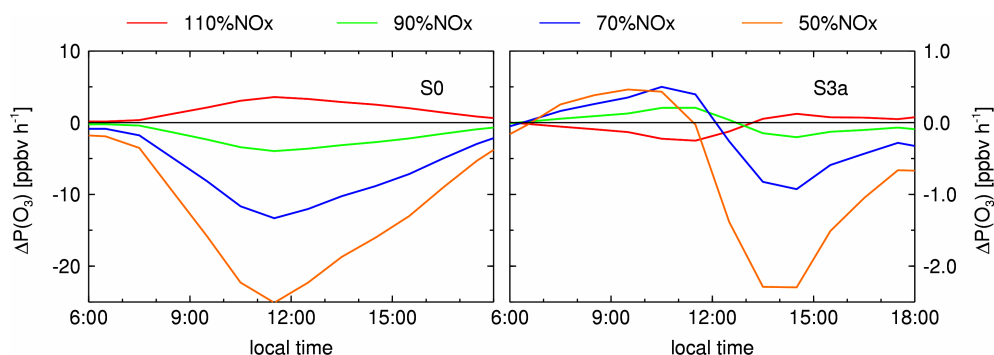

Fig. 10. Hourly $\Delta P(O_3)$ due to NO_x changes under S0 and S3a.

An implication from Figure 9 is that concurrent reduction of both NO_x and VOCs only gives limited additional $P(O_3)$ reduction than reducing one of them based on near-surface modeling analysis. For example, $\Delta P(O_3)_{NO+VOCs}$ from 50 % reductions of both NO_x and VOC is only 20 % more than $\Delta P(O_3)_{VOCs}$ of 50 % reduction in VOC (Fig. 9d for S1b). Under the most likely scenario (with excess HONO and aromatics) based on the in situ observations, reducing either NO_x or VOCs can be effective.

Since the surface concentrations are constrained by the observations and turbulent mixing in the PBL is based on the WRF simulation, we show selected REAM-1D simulation results with and without aromatics (S0 and S2) in the Supplement to examine if the PBL-integrated $P(O_3)$ shows similar characteristics as near the surface. Figure S2 in the Supplement shows a rapid decrease of O_3 production rates with altitude, due to the reduced NO_x and (to a lesser degree) VOCs. Column $P(O_3)$ integrated from the surface to the top of the

Table 2. R^2 values beteewn $P(O_3)$ and $\sqrt{Q - L_N - L_R}[NO]$, $\frac{L_{OH-VOC}}{L_{OH-NO_2}}(Q - 2PER - L_R - L_{ON})$, Q, and NO during the daytime (06:00–18:00) and afteroon (12:00–18:00).

	$\sqrt{Q - L_N - L_R}$ [NO]		$\frac{L_{OH-VOC}}{L_{OH-NO_2}}(Q - 2PER - L_R - L_{ON})$		Q		NO	
	day	afternoon	day	afternoon	day	afternoon	day	afternoon
S0	0.19	0.5	0.79	0.79	0.74	0.66	0.002	0.2
S0a	0.18	0.56	0.49	0.49	0.79	0.72	0.002	0.18
S0b	0.2	0.34	0.72	0.77	0.58	0.46	0.002	0.14
S1	0.09	0.69	0.77	0.77	0.86	0.85	0.03	0.09
S2	0.14	0.26	0.77	0.79	0.49	0.34	0.01	0.06
S3	0.1	0.59	0.76	0.79	0.77	0.72	0.07	0.03
S3a	0.06	0.56	0.76	0.77	0.62	0.79	0.08	0.03

PBL shows similar dependence to the change of NO_x and VOCs as in Fig. 9, although the column $P(O_3)$-VOC sensitivity is weaker than near the surface and is similar to column $P(O_3)$-NO_x sensitivity. Inspection of model results suggests that the O_3 production chemical regime increasingly shifts toward being NO_x-limited away from the surface (Fig. S4 in the Supplement). The co-benefit of concurrent reduction of both NO_x and VOCs in reducing O_3 production is larger when integrated in the PBL column than near the surface (by comparing Fig. S4 of the Supplement with Figure 9).

3.4.2 Evaluation with diagnostic equations of O_3 production for different chemical regimes

Various studies have provided relatively simple diagnostics for O_3 production regimes (e.g. Sillman et al., 1990; Kleinman et al., 1997; Daum et al., 2000). Lei et al. (2007) summarized these studies into two equations:

$$NO_x - \text{limited regime}, P(O_3) \quad (1)$$
$$= Y \frac{k_t}{\sqrt{2k_{\text{eff}}}}\sqrt{Q - L_N - L_R}[NO]$$

$$VOC - \text{limited regime}, P(O_3) \quad (2)$$
$$= Y \frac{L_{OH-VOC}}{L_{OH-NO_2}}(Q - 2PER - L_R - L_{ON})$$

where k_t is the weighted average rate constant for reaction of HO_2 and RO_2 with NO; k_{eff} is the effective rate constant for peroxide (H_2O_2 and ROOH) formation; Q is the total primary source of RO_x radicals, in ppbv h^{-1}; L_N, L_R and L_{ON} are the radical loss rates due to the reactions of OH + HO_2, RO_2 + R'O_2, and radical-NO_x reactions excluding OH + NO_2, respectively; Y is the average yield of HO_2 and RO_2 for each OH + VOC reaction; L_{OH-VOC} and L_{OH-NO_2} are the loss rates of OH due to reactions with VOCs and NO_2, respectively; PER is the peroxide formation rate.

We compare the correlations between model calculated hourly $P(O_3)$ (ppbv h^{-1}) and those from the diagnostic equations (Lei et al., 2007). The results for different model sensi-

tivity simulations are shown in Table 2. We also show in Table 2 the correlations with NO and the primary RO_x source Q. In the standard model (S0), $P(O_3)$ shows better correlation with $\frac{L_{OH-VOC}}{L_{OH-NO_2}}(Q - 2PER - L_R - L_{ON})$ (afternoon $R^2 = 0.79$; daytime $R^2 = 0.79$) than with the NO_x-limited diagnostics ($\sqrt{Q - L_N - L_R}$ [NO]) (afternoon $R^2 = 0.50$; daytime $R^2 = 0.19$), mainly due to the much better $P(O_3)$-Q correlation (afternoon $R^2 = 0.66$; daytime $R^2 = 0.74$) than the $P(O_3)$-NO correlation (afternoon $R^2 = 0.22$; daytime $R^2 = 0.002$). These suggest that $P(O_3)$ during our observations in Beijing behave more like in the VOC-limited regime than the NO_x-limited regime. This is particularly true when morning data are taken into account since O_3 production can clearly reside in the VOC-limited regime (Fig. 10). It is interesting to note that the VOC-limited regime in the morning disappears when the sensitivity is integrated in the PBL (Fig. S5 in the Supplement). In the afternoon when O_3 production is large, however, both diagnostics show reasonably good correlations with the $P(O_3)$. An outlier is the scenario of S2 when aromatics are not included; the chemical regime clearly shifts into the VOC-limited regime given the much better correlation ($R^2 = 0.79$) with $\frac{L_{OH-VOC}}{L_{OH-NO_2}(Q-2PER-L_R-L_{ON})}$ than with ($\sqrt{Q - L_N - L_R}$ [NO]) ($R^2 = 0.26$). In the scenario of S0a (without HO_2 aerosol uptake) for the afternoon, $P(O_3)$ correlate even better with the NO_x-limited diagnostics ($R^2 = 0.56$) than with the VOC-limited diagnostics ($R^2 = 0.49$). Comparing the results of S0, S0a, and S0b, aerosol uptake of HO_2 tends to shift the O_3 production more towards the VOC-limited regime.

In general, the diagnostic equations are consistent with our sensitivity simulations, suggesting that under the most realistic scenario (S0), O_3 production in Beijing is in the transition regime. Aromatics and excess HONO tend to shift O_3 production into NO_x-limited regime, while aerosol HO_2 sink tends to shift it towards VOC-limited regime.

4 Conclusions

In this work, summertime photochemistry at Beijing is investigated with a 1-D photochemical model constrained by the observations near the surface. Through detailed chemical budget analysis, we find that VOC (especially aromatics) oxidation and heterogeneous chemistry (including HONO formation and HO_2 uptake by aerosols) play potentially critical roles in RO_x budgets and O_3 formation. A series of modeling experiments are conducted to explore the model sensitivities to these processes, particularly in light of the uncertainties in the understanding of heterogeneous processes. Although the quantitative results presented are somewhat dependent on the parameters we chose for the heterogeneous reactions, the detailed diagnostics of radical sources and sinks and model sensitivity results can be used to estimate the significance of these processes when better information is available or alternative assumptions are made in future studies. Sensitivity experiments are also done for determining the response of $P(O_3)$ to the change of NO_x and VOCs in order to understand the O_3 photochemical regimes near the surface.

Through a detailed chemical budget analysis, we find that summertime photochemistry in Beijing is characterized by fast formation, recycling and removal of RO_x radicals. The total RO_x primary source (and sink) ($6.6\,ppbv\,h^{-1}$) near the surface in Beijing is close to the largest values reported for urban environments. Photolysis of OVOCs ($4.2\,ppbv\,h^{-1}$) and excess HONO ($2.2\,ppbv\,h^{-1}$) are the two largest RO_x sources, much more important than that from O^1D+H_2O ($0.4\,ppbv\,h^{-1}$). Formation of RO_2NO_2 ($1.0\,ppbv\,h^{-1}$) and $RONO_2$ ($0.7\,ppbv\,h^{-1}$) are as important as the typical major RO_x sink via $OH+NO_2$ reaction ($1.6\,ppbv\,h^{-1}$). Aromatics are the major player in OVOC and organic nitrate formation. Aerosol uptake of HO_2 may also be a major RO_x sink due to the large aerosol surface area in Beijing, and this sink is quite sensitive to the value of $\gamma\,(HO_2)$. The importance of aromatics, heterogeneous HONO production, and possibly large aerosol update of HO_2 signifies the unique photochemical environments in Beijing. These characteristics are likely to be present over many regions of the polluted eastern China with large clusters of cities and industrial regions. Observation-based modeling studies of RO_x radical chemistry over these regions that include high quality comprehensive measurements of RO_x radicals, HONO, organic nitrates, and VOCs (aromatics in particular) and their oxidation products will be necessary to reduce the uncertainties of the factors discussed in this study and develop more accurate mechanistic and quantitative understanding of the photochemical system.

The chemical production of O_3 near the surface in Beijing is extremely fast, at $32\,ppbv\,h^{-1}$ on average during daytime. The high concentrations of NO ($\sim 5\,ppbv$ at noontime), excess HONO and aromatic VOCs are the major driving factors. The O_3 production rate decreases rapidly away from the surface in the PBL, leading to a factor of 4 lower gross

and net O_3 production rates in the PBL compared to the surface. The chemical loss of O_3 near the surface is also fast, about $6\,ppbv\,h^{-1}$, and the heterogeneous formation of excess HONO via $NO_2 \rightarrow HONO$ is actually the largest ($\sim 40\,\%$) O_3 loss term. Sensitivity simulations and analysis using diagnostic equations suggest that the O_3 production in Beijing does not lie in either the VOC-limited regime or in the NO_x-limited regime, but in the transition regime, where reduction of either NO_x or VOCs could lead to reduced O_3 production. The transition regime feature is even more pronounced than near the surface when the sensitivity to NO_x or VOCs of column $P(O_3)$ rate integrated from the surface to the top of the PBL is considered. It implies that there is flexibility in choosing either NO_x or VOC reduction to achieve the most cost-effective O_3 reduction. The co-benefit of concurrent reduction of both NO_x and VOCs is small based on modeling analysis of near-surface observations. However, it becomes significant when integrated in the PBL column.

In this study, we have focused on understanding the photochemistry using observation-constrained modeling. Our results point to chemical characteristics not yet well represented in current 3-D modeling studies. The large clustering of concentrated city and industrial regions in the eastern China, such as North China Plain (NCP), Yangtze River Delta (YRD), and PRD, suggests that fast photochemistry plays a critically important role in determining O_3 levels in these regions. 3-D modeling analysis, ideally constrained by in situ or remote sensing observations, will be necessary to understand the interplay of chemistry and transport on the regional and global scales.

References

Acker, K., Febo, A., Trick, S., Perrino, C., Bruno, P., Wiesen, P., Moller, D., Wieprecht, W., Auel, R., Giusto, M., Geyer, A., Platt, U., and Allegrini, I.: Nitrous acid in the urban area of Rome, Atmos. Environ., 40, 3123–3133, doi:10.1016/j.atmosenv.2006.01.028, 2006.

Amoroso, A., Beine, H. J., Sparapani, R., Nardino, M., and Allegrini, I.: Observation of coinciding arctic boundary layer ozone depletion and snow surface emissions of nitrous acid, Atmos. Environ., 40, 1949–1956, 2006.

An, J. L., Zhang, W., and Qu, Y.: Impacts of a strong cold front on concentrations of HONO, HCHO, O_3, and NO_2 in the heavy traffic urban area of Beijing, Atmos. Environ., 43, 3454–3459, doi:10.1016/j.atmosenv.2009.04.052, 2009.

Carter, W. P. L.: Development of the SAPRC–07 chemical mechanism and upadated ozone reactivity scales. Final Report to the California Air Resources Board Contract No. 03-318, 2009.

Cermak, J. and Knutti, R.: Beijing Olympics as an aerosol field experiment, Geophys. Res. Lett., 36, L10806, doi:10.1029/2009GL038572, 2009.

Chan, C. K. and Yao, X.: Air pollution in mega cities in China, Atmos. Environ., 42, 1–42, doi:10.1016/j.atmosenv.2007.09.003, 2008.

Choi, Y., Wang, Y. H., Zeng, T., Martin, R. V., Kurosu, T. P., and Chance, K.: Evidence of lightning NO_x and convective transport of pollutants in satellite observations over North America, Geophys. Res. Lett., 32, L02805, doi:10.1029/2004gl021436, 2005.

Choi, Y., Wang, Y., Zeng, T., Cunnold, D., Yang, E. S., Martin, R., Chance, K., Thouret, V., and Edgerton, E.: Springtime transitions of NO_2, CO, and O-3 over North America: Model evaluation and analysis, J. Geophys. Res.-Atmos., 113, D20311, doi:10.1029/2007JD009632, 2008a.

Choi, Y., Wang, Y. H., Yang, Q., Cunnold, D., Zeng, T., Shim, C., Luo, M., Eldering, A., Bucsela, E., and Gleason, J.: Spring to summer northward migration of high O-3 over the western North Atlantic, Geophys. Res. Lett., 35, L04818, doi:10.1029/2007GL032276, 2008b.

Chou, C. C. K., Tsai, C. Y., Shiu, C. J., Liu, S. C., and Zhu, T.: Measurement of NO_y during Campaign of Air Quality Research in Beijing 2006 (CAREBeijing-2006): Implications for the ozone production efficiency of NO_x, J. Geophys. Res.-Atmos., 114, D00G01, doi:10.1029/2008jd010446, 2009.

Chou, C. C. K., Tsai, C. Y., Chang, C. C., Lin, P. H., Liu, S. C., and Zhu, T.: Photochemical production of ozone in Beijing during the 2008 Olympic Games, Atmos. Chem. Phys., 11, 9825–9837, doi:10.5194/acp-11-9825-2011, 2011.

Costabile, F., Amoroso, A., and Wang, F.: Sub-mu m particle size distributions in a suburban Mediterranean area. Aerosol populations and their possible relationship with HONO mixing ratios, Atmos. Environ., 44, 5258–5268, doi:10.1016/j.atmosenv.2010.08.018, 2010.

Daum, P. H., Kleinman, L. I., Imre, D. G., Nunnermacker, L. J., Lee, Y.-N., Springston, S. R., Newman, L., and Weinstein-Lloyd, J.: Analysis of the processing of Nashville urban emissions on July 3 and July 18, 1995, J. Geophys. Res., 105, 9155–9164, 2000.

Dusanter, S., Vimal, D., Stevens, P. S., Volkamer, R., Molina, L. T., Baker, A., Meinardi, S., Blake, D., Sheehy, P., Merten, A., Zhang, R., Zheng, J., Fortner, E. C., Junkermann, W., Dubey, M., Rahn, T., Eichinger, B., Lewandowski, P., Prueger, J., and Holder, H.: Measurements of OH and HO_2 concentrations during the MCMA-2006 field campaign – Part 2: Model comparison and radical budget, Atmos. Chem. Phys., 9, 6655–6675, doi:10.5194/acp-9-6655-2009, 2009.

Elshorbany, Y. F., Kurtenbach, R., Wiesen, P., Lissi, E., Rubio, M., Villena, G., Gramsch, E., Rickard, A. R., Pilling, M. J., and Kleffmann, J.: Oxidation capacity of the city air of Santiago, Chile, Atmos. Chem. Phys., 9, 2257–2273, 10, http://www.atmos-chem-phys.net/9/2257/10/.5194/acp-9-2257-2009, 2009.

Emmerson, K. M., Carslaw, N., Carpenter, L. J., Heard, D. E., Lee, J. D., and Pilling, M. J.: Urban atmospheric chemistry during the PUMA campaign 1: Comparison of modelled OH and HO2 concentrations with measurements, J. Atmos. Chem., 52, 143–164, doi:10.1007/s10874-005-1322-3, 2005a.

Emmerson, K. M., Carslaw, N., and Pilling, M. J.: Urban atmospheric chemistry during the PUMA campaign 2: Radical budgets for OH, HO_2 and RO_2, J. Atmos. Chem., 52, 165–183, doi:10.1007/s10874-005-1323-2, 2005b.

Farmer, D. K., Perring, A. E., Wooldridge, P. J., Blake, D. R., Baker, A., Meinardi, S., Huey, L. G., Tanner, D., Vargas, O., and Cohen, R. C.: Impact of organic nitrates on urban ozone production, Atmos. Chem. Phys., 11, 4085–4094, doi:10.5194/acp-11-4085-2011, 2011.

Haagen-Smit, A. J. and Fox, M. M.: Photochemical ozone formation with hydrocarbons and automobile exhaust, J. Air Pollut. Control Assoc., 4, 105–109, 1954.

Hecobian, A., Liu, Z., Hennigan, C. J., Huey, L. G., Jimenez, J. L., Cubison, M. J., Vay, S., Diskin, G. S., Sachse, G. W., Wisthaler, A., Mikoviny, T., Weinheimer, A. J., Liao, J., Knapp, D. J., Wennberg, P. O., Kürten, A., Crounse, J. D., Clair, J. St., Wang, Y., and Weber, R. J.: Comparison of chemical characteristics of 495 biomass burning plumes intercepted by the NASA DC-8 aircraft during the ARCTAS/CARB-2008 field campaign, Atmos. Chem. Phys., 11, 13325–13337, doi:10.5194/acp-11-13325-2011, 2011.

Ho, S. S. H. and Yu, J. Z.: Determination of airborne carbonyls: Comparison of a thermal desorption/GC method with the standard DNPH/HPLC method, Environ. Sci. Technol., 38, 862–870, doi:10.1021/es034784w, 2004.

Hofzumahaus, A., Rohrer, F., Lu, K. D., Bohn, B., Brauers, T., Chang, C. C., Fuchs, H., Holland, F., Kita, K., Kondo, Y., Li, X., Lou, S. R., Shao, M., Zeng, L. M., Wahner, A., and Zhang, Y. H.: Amplified Trace Gas Removal in the Troposphere, Science, 324, 1702–1704, doi:10.1126/science.1164566, 2009.

Jenkin, M. E., and Clemitshaw, K. C.: Ozone and other secondary photochemical pollutants: chemical processes governing their formation in the planetary boundary layer, Atmos. Environ., 34, 2499–2527, doi:10.1016/s1352-2310(99)00478-1, 2000.

Kanaya, Y., Fukuda, M., Akimoto, H., Takegawa, N., Komazaki, Y., Yokouchi, Y., Koike, M., and Kondo, Y.: Urban photochemistry in central Tokyo: 2. Rates and regimes of oxidant ($O_3 + NO_2$) production, J. Geophys. Res.-Atmos., 113, D06301, doi:10.1029/2007jd008671, 2008.

Kanaya, Y., Pochanart, P., Liu, Y., Li, J., Tanimoto, H., Kato, S., Suthawaree, J., Inomata, S., Taketani, F., Okuzawa, K., Kawamura, K., Akimoto, H., and Wang, Z. F.: Rates and regimes of photochemical ozone production over Central East China in June 2006: a box model analysis using comprehensive measurements of ozone precursors, Atmos. Chem. Phys., 9, 7711–7723, doi:10.5194/acp-9-7711-2009, 2009.

Kleffmann, J.: Daytime sources of nitrous acid (HONO) in the atmospheric boundary layer, Chem. Phys. Chem., 8, 1137–1144, doi:10.1002/cphc.200700016, 2007.

Kleinman, L. I., Daum, P. H., Lee, J. H., Lee, Y.-N., Nunnermacker, L. J., Springston, S. R., Newman, L., Weinstein-Lloyd, J., and Sillman, S.: Dependence of ozone production on NO and hydrocarbons in the troposphere, Geophys. Res. Lett., 24, 2299–2302, 1997.

Lei, W., de Foy, B., Zavala, M., Volkamer, R., and Molina, L. T.: Characterizing ozone production in the Mexico City Metropolitan Area: a case study using a chemical transport model, Atmos. Chem. Phys., 7, 1347–1366, doi:10.5194/acp-7-1347-2007, 2007

Lin, J.-T., Liu, Z., Zhang, Q., Liu, H., Mao, J., and Zhuang, G.: Model uncertainties affecting satellite-based inverse modeling of nitrogen oxides emissions and implications for surface ozone simulation, Atmos. Chem. Phys. Discuss., 12, 14269–14327, doi:10.5194/acpd-12-14269-2012, 2012.

Liu, S. C., Trainer, M., Fehsenfeld, F. C., Parrish, D. D., Williams, E. J., Fahey, D. W., Hübler, G., and Murphy, P. C.: Ozone Production in the Rural Troposphere and the Implications for Regional and Global Ozone Distributions, J. Geophys. Res., 92, 4191–4207, 1987.

Liu, Z., Wang, Y. H., Gu, D. S., Zhao, C., Huey, L. G., Stickel, R., Liao, J., Shao, M., Zhu, T., Zeng, L. M., Liu, S. C., Chang, C. C., Amoroso, A., and Costabile, F.: Evidence of Reactive Aromatics As a Major Source of Peroxy Acetyl Nitrate over China, Environ. Sci. Technol., 44, 7017–7022, doi:10.1021/es1007966, 2010.

Liu, Z., Wang, Y. H., Vrekoussis, M., Richter, A., Wittrock, F., Burrows, J. P., Shao, M., Chang, C.-C., Liu, S.-C., Wang, H., and Chen. C.: Exploring the missing source of glyoxal (CHOCHO) over China, Geophys. Res. Lett., 39, L10812, doi:10.1029/2012GL051645, 2012.

Lou, S., Holland, F., Rohrer, F., Lu, K., Bohn, B., Brauers, T., Chang, C. C., Fuchs, H., Häseler, R., Kita, K., Kondo, Y., Li, X., Shao, M., Zeng, L., Wahner, A., Zhang, Y., Wang, W., and Hofzumahaus, A.: Atmospheric OH reactivities in the Pearl River Delta – China in summer 2006: measurement and model results, Atmos. Chem. Phys., 10, 11243–11260, 10, http://www.atmos-chem-phys.net/10/11243/10/.5194/acp-10-11243-2010, 2010.

Lu, K. D., Rohrer, F., Holland, F., Fuchs, H., Bohn, B., Brauers, T., Chang, C. C., Häseler, R., Hu, M., Kita, K., Kondo, Y., Li, X., Lou, S. R., Nehr, S., Shao, M., Zeng, L. M., Wahner, A., Zhang, Y. H., and Hofzumahaus, A.: Observation and modelling of OH and HO2 concentrations in the Pearl River Delta 2006: a missing OH source in a VOC rich atmosphere, Atmos. Chem. Phys., 12, 1541–1569, doi:10.5194/acp-12-1541-2012, 2012.

Mao, J., Jacob, D. J., Evans, M. J., Olson, J. R., Ren, X., Brune, W. H., Clair, J. M. S., Crounse, J. D., Spencer, K. M., Beaver, M. R., Wennberg, P. O., Cubison, M. J., Jimenez, J. L., Fried, A., Weibring, P., Walega, J. G., Hall, S. R., Weinheimer, A. J., Cohen, R. C., Chen, G., Crawford, J. H., McNaughton, C., Clarke, A. D., Jaeglé, L., Fisher, J. A., Yantosca, R. M., Le Sager, P., and Carouge, C.: Chemistry of hydrogen oxide radicals (HO$_x$) in the Arctic troposphere in spring, Atmos. Chem. Phys., 10, 5823–5838, doi:10.5194/acp-10-5823-2010, 2010.

Molina, M. J. and Molina, L. T.: Megacities and atmospheric pollution, J. Air Waste Manage. Assoc., 54, 644–680, 2004.

Monks, P. S., Granier, C., Fuzzi, S., Stohl, A., Williams, M. L., Akimoto, H., Amann, M., Baklanov, A., Baltensperger, U., Bey, I., Blake, N., Blake, R. S., Carslaw, K., Cooper, O. R., Dentener, F., Fowler, D., Fragkou, E., Frost, G. J., Generoso, S., Ginoux, P., Grewe, V., Guenther, A., Hansson, H. C., Henne, S., Hjorth, J., Hofzumahaus, A., Huntrieser, H., Isaksen, I. S. A., Jenkin, M. E., Kaiser, J., Kanakidou, M., Klimont, Z., Kulmala, M., Laj, P., Lawrence, M. G., Lee, J. D., Liousse, C., Maione, M., McFiggans, G., Metzger, A., Mieville, A., Moussiopoulos, N., Orlando,

J. J., O'Dowd, C. D., Palmer, P. I., Parrish, D. D., Petzold, A., Platt, U., Poschl, U., Prevot, A. S. H., Reeves, C. E., Reimann, S., Rudich, Y., Sellegri, K., Steinbrecher, R., Simpson, D., ten Brink, H., Theloke, J., van der Werf, G. R., Vautard, R., Vestreng, V., Vlachokostas, C., and von Glasow, R.: Atmospheric composition change – global and regional air quality, Atmos. Environ., 43, 5268–5350, doi:10.1016/j.atmosenv.2009.08.021, 2009.

NARSTO: An assessment of tropospheric ozone pollution – A North American perspective. NARSTO Management Office (Envair), Pasco, Washington, USA, available at: http://narsto.org/, (last access: 5/10/2006), 2000.

NARSTO: Improving emission inventories for effective Air Quality Management Across North America, NARSTO 05-001, Pasco, Washington, USA, 2005.

NRC (National Research Council): Rethinking the ozone problem in urban and regional air pollution, National Academy Press, Washington, DC, USA, 1991.

Pathak, R. K., Wu, W. S., and Wang, T.: Summertime PM$_{2.5}$ ionic species in four major cities of China: nitrate formation in an ammonia-deficient atmosphere, Atmos. Chem. Phys., 9, 1711–1722, doi:10.5194/acp-9-1711-2009, 2009.

Pinto, J. P., Meng, Q., Dibb, J. E., Lefer, B. L., Rappenglueck, B., Ren, X., Stutz, J., and Zhang, R.: Intercomparison of nitrous acid (HONO) measurement techniques during SHARP, AGU fall meeting, San Fransisco, USA, 2010.

Ren, X. R., Harder, H., Martinez, M., Lesher, R. L., Oliger, A., Simpas, J. B., Brune, W. H., Schwab, J. J., Demerjian, K. L., He, Y., Zhou, X. L., and Gao, H. G.: OH and HO2 chemistry in the urban atmosphere of New York City, Atmos. Environ., 37, 3639–3651, doi:10.1016/s1352-2310(03)00459-x, 2003.

Richter, A., Burrows, J. P., Nuss, H., Granier, C., and Niemeier, U.: Increase in tropospheric nitrogen dioxide over China observed from space, Nature, 437, 129–132, doi:10.1038/nature04092, 2005.

Ryerson, T. B., Williams, E. J., and Fehsenfeld, F. C.: An efficient photolysis system for fast-response NO$_2$ measurements, J. Geophys. Res.-Atmos., 105, 26447–26461, 2000.

Sander, S. P., Abbatt, J., Barker, J. R., Burkholder, J. B., Friedl, R. R., Golden, D. M., Huie, R. E., Kolb, C. E., Kurylo, M. J., Moortgat, G. K., Orkin, V. L., and Wine, P. H.: Chemical Kinetics and Photochemical Data for Use in Atmospheric Studies, Evaluation No. 17, JPL Publication 10-6, Jet Propulsion Laboratory, Pasadena, CA, USA, available at: http://jpldataeval.jpl.nasa.gov, 2011.

Shao, M., Lu, S. H., Liu, Y., Xie, X., Chang, C. C., Huang, S., and Chen, Z. M.: Volatile organic compounds measured in summer in Beijing and their role in ground-level ozone formation, J. Geophys. Res.-Atmos., 114, D00G06, doi:10.1029/2008jd010863, 2009.

Shirley, T. R., Brune, W. H., Ren, X., Mao, J., Lesher, R., Cardenas, B., Volkamer, R., Molina, L. T., Molina, M. J., Lamb, B., Velasco, E., Jobson, T., and Alexander, M.: Atmospheric oxidation in the Mexico City Metropolitan Area (MCMA) during April 2003, Atmos. Chem. Phys., 6, 2753–2765, doi:10.5194/acp-6-2753-2006, 2006.

Sillman, S., Logan, J. A., and Wofsy, S. C.: The sensitivity of ozone to nitrogen oxides and hydrocarbons in regional ozone episodes, J. Geophys. Res., 95, 1837–1851, 1990.

Slusher, D. L., Huey, L. G., Tanner, D. J., Flocke, F. M., and Roberts, J. M.: A thermal dissociation-chemical ionization mass spectrometry (TD-CIMS) technique for the simultaneous measurement of peroxyacyl nitrates and dinitrogen pentoxide, J. Geophys. Res.-Atmos., 109, D19315, doi:10.1029/2004jd004670, 2004.

Streets, D. G., Fu, J. S., Jang, C. J., Hao, J. M., He, K. B., Tang, X. Y., Zhang Y. H., Wang, Z. F., Li, Z. P., Zhang, Q., Wang, L. T., Wang, B. Y., and Yu, C.: Air quality during the 2008 Beijing Olympic Games, Atmos. Environ., 41, 480–492, 2008.

Su, H., Cheng, Y. F., Shao, M., Gao, D. F., Yu, Z. Y., Zeng, L. M., Slanina, J., Zhang, Y. H., and Wiedensohler, A.: Nitrous acid (HONO) and its daytime sources at a rural site during the 2004 PRIDE-PRD experiment in China, J. Geophys. Res.-Atmos., 113, D14312, doi:10.1029/2007jd009060, 2008.

Su, H., Cheng, Y., Oswald, R., Behrendt, T., Trebs, I., Meixner, F. X., Andreae, M. O., Cheng, P., Zhang, Y., Pöschl, U.: Soil Nitrite as a Source of Atmospheric HONO and OH Radicals, Science, 333, 1616–1618, 2011.

Taketani, F., Kanaya, Y., Pochanart, P., Liu, Y., Li, J., Okuzawa, K., Kawamura, K., Wang, Z., and Akimoto, H.: Measurement of overall uptake coefficients for HO_2 radicals by aerosol particles sampled from ambient air at Mts. Tai and Mang, China, Atmos. Chem. Phys. Discuss., 12, 13787–13812, doi:10.5194/acpd-12-13787-2012, 2012.

Thornton, J. and Abbatt, J. P. D.: Measurements of HO_2 uptake to aqueous aerosol: Mass accommodation coefficients and net reactive loss, J. Geophys. Res.-Atmos., 110, D08309, doi:10.1029/2004jd005402, 2005.

Thornton, J. A., Jaegle, L., and McNeill, V. F.: Assessing known pathways for HO_2 loss in aqueous atmospheric aerosols: Regional and global impacts on tropospheric oxidants, J. Geophys. Res.-Atmos., 113, D05303, doi:10.1029/2007jd009236, 2008.

Trainer, M., Buhr, M. P., Curran, C. M., Fehsenfeld, F. C., Hsie, E. Y., Liu, S. C., Norton, N. B., Parrish, D. D., Williams, E. J., Gandrud, B. W., Ridley, B. A., Shetter, J. D., Allwine, E. J., and Westberg, H. H.: Observations and Modeling of the Reactive Nitrogen Photochemistry at a Rural Site, J. Geophys. Res., 96, 3045–3063, 1991.

van Donkelaar, A., Martin, R. V., Brauer, M., Kahn, R., Levy, R., Verduzco, C., and Villeneuve, P. J.: Global Estimates of Ambient Fine Particulate Matter Concentrations from Satellite-Based Aerosol Optical Depth: Development and Application, Environ. Health Perspect., 118, 847–855, doi:10.1289/ehp.0901623, 2010.

Volkamer, R., Sheehy, P., Molina, L. T., and Molina, M. J.: Oxidative capacity of the Mexico City atmosphere – Part 1: A radical source perspective, Atmos. Chem. Phys., 10, 6969–6991, doi:10.5194/acp-10-6969-2010, 2010.

Wang, T., Nie, W., Gao, J., Xue, L. K., Gao, X. M., Wang, X. F., Qiu, J., Poon, C. N., Meinardi, S., Blake, D., Wang, S. L., Ding, A. J., Chai, F. H., Zhang, Q. Z., and Wang, W. X.: Air quality during the 2008 Beijing Olympics: secondary pollutants and regional impact, Atmos. Chem. Phys., 10, 7603–7615, doi:10.5194/acp-10-7603-2010, 2010.

Wood, E. C., Herndon, S. C., Onasch, T. B., Kroll, J. H., Canagaratna, M. R., Kolb, C. E., Worsnop, D. R., Neuman, J. A., Seila, R., Zavala, M., and Knighton, W. B.: A case study of ozone production, nitrogen oxides, and the radical budget in Mexico City, Atmos. Chem. Phys., 9, 2499–2516, doi:10.5194/acp-9-2499-2009, 2009.

Yang, Q., Wang, Y. H., Zhao, C., Liu, Z., Gustafson, W. I. J., and Shao, M.: NO_x emission reduction and its effects on ozone during the 2008 Olympic Games, Environ. Sci. Technol., 45, 6404–6410. doi:10.1021/es200675v, 2011.

Zhang, Q., Streets, D. G., Carmichael, G. R., He, K. B., Huo, H., Kannari, A., Klimont, Z., Park, I. S., Reddy, S., Fu, J. S., Chen, D., Duan, L., Lei, Y., Wang, L. T., and Yao, Z. L.: Asian emissions in 2006 for the NASA INTEX-B mission, Atmos. Chem. Phys., 9, 5131–5153, doi:10.5194/acp-9-5131-2009, 2009.

Zhang, Y. H., Su, H., Zhong, L. J., Cheng, Y. F., Zeng, L. M., Wang, X. S., Xiang, Y. R., Wang, J. L., Gao, D. F., Shao, M., Fan, S. J., and Liu, S. C.: Regional ozone pollution and observation-based approach for analyzing ozone-precursor relationship during the PRIDE-PRD2004 campaign, Atmos. Environ., 42, 6203–6218, doi:10.1016/j.atmosenv.2008.05.002, 2008.

Zhao, C., Wang, Y. H., and Zeng, T.: East China Plains: A "Basin" of Ozone Pollution, Environ. Sci. Technol., 43, 1911–1915, doi:10.1021/ES8027764, 2009a.

Zhao, C., Wang, Y., Choi, Y., and Zeng, T.: Summertime impact of convective transport and lightning NO_x production over North America: modeling dependence on meteorological simulations, Atmos. Chem. Phys., 9, 4315–4327, 2009b, http://www.atmos-chem-phys.net/9/4315/2009/.

Zhao, C. and Wang, Y. H.: Assimilated inversion of NO_x emissions over east Asia using OMI NO2 column measurements, Geophys. Res. Lett., 36, L06805, doi:10.1029/2008gl037123, 2009.

Zhao, C., Wang, Y. H., Yang, Q., Fu, R., Cunnold, D., and Choi, Y.: Impact of East Asian summer monsoon on the air quality over China: View from space, J. Geophys. Res.-Atmos., 115, D09301, doi:10.1029/2009jd012745, 2010.

Zhu, T., Li, X., Hu, M., Tang, X., Team, CareBeijing.:Air pollution characteristics before, during, and after the Beijing Olympics, Epidemiology, 20, S250, doi:10.1097/01.ede.0000362836.37333.86, 2009.